Determination of spin pumping as a source of linewidth in sputtered $Co_{90}Fe_{10}$/Pd multilayers by use of broadband ferromagnetic resonance spectroscopy

Justin M. Shaw,* Hans T. Nembach, and T. J. Silva
National Institute of Standards and Technology, Boulder, CO 80305, USA
(Received 28 October 2011; revised manuscript received 22 December 2011; published 10 February 2012)

We performed a systematic study of damping in $Co_{90}Fe_{10}$/Pd multilayers by use of broadband (1–60 GHz) ferromagnetic resonance (FMR) spectroscopy in the perpendicular geometry. The data were fitted with the conventional Landau-Lifshitz equation in conjunction with an inhomogeneous contribution to linewidth ΔH_0. Samples were prepared with net perpendicular anisotropy field values ranging from -0.5 to $+1.2$ T. ΔH_0 shows a dependence on the perpendicular anisotropy, though the Landau-Lifshitz damping parameter α, which ranged from 0.016 to 0.04, exhibits no trend as a function of anisotropy. We explain the wide variation of α as a result of spin pumping from $Co_{90}Fe_{10}$ into adjacent nonmagnetic layers. We use a quantitative model for spin pumping that includes the intrinsic spin-mixing conductance at the $Co_{90}Fe_{10}$/Pd interface and the spin-diffusion length of Pd, which were experimentally measured at room temperature to be $(1.07 \pm 0.13) \times 10^{19}$ m^{-2} and 8.6 ± 1.0 nm, respectively. We quantitatively show how α is enhanced by spin pumping through an FMR investigation of individual Pd/CoFe/Pd, and Pd/CoFe/Pd/CoFe/Pd layer structures.

DOI: 10.1103/PhysRevB.85.054412 PACS number(s): 75.30.Ds, 75.70.Cn, 76.50.+g

I. INTRODUCTION

Magnetic multilayer materials with strong perpendicular magnetic anisotropy are amenable for use in emerging spintronics[1,2] and next-generation data-storage technologies[3] due to the high degree of tunability of both the anisotropy and saturation magnetization. Such multilayers can be formed from alternating two ferromagnetic materials such as Co/Ni[4] and CoFe/Ni,[5] or alternating a ferromagnetic material with a nonferromagnetic material such as Co/Pt,[6–9] Co/Pd,[10] CoFe/Pd,[11] and CoNi/Pt.[12] The high-frequency behavior of these materials is of considerable technological interest due to the strong dependence of spin-torque critical currents and patterned-media switching rates on the degree of damping for gyromagnetic precession.[13] However, measurements of damping in multilayers by use of ferromagnetic resonance (FMR) can be challenging in the case of strong perpendicular anisotropies (which require high measurement frequencies in excess of 30 GHz) and/or broad ferromagnetic resonance (FMR) linewidths (which necessitate high instrument signal-to-noise ratio [nr] and stability).

We recently reported that the measured Landau-Lifshitz (LL) damping parameter α of $Co_{90}Fe_{10}$/Ni multilayers is an average of the values for α in the individual constituent layers weighted by the relative spin densities of the constituents.[5] In that case, the multilayers were composed of alternating ferromagnetic layers. This raises the question: What determines α when one of the multilayer constituents is a nonmagnetic material such as Pt or Pd?

To date, many studies have shown that α can be enhanced in single ferromagnetic layers as well as bilayers and pseudo–spin-valve structures.[14–23] Such studies highlight the influence of spin pumping on the damping process in samples that consist of multiple layers and materials. However, the role of spin pumping in multilayers with perpendicular anisotropy has yet to be thoroughly addressed.

Previous studies of precessional dynamics in Co/Pd and Co/Pt reported values of α as large as 0.2.[24–26] However, for all of these previous studies, linewidths were measured at a single frequency or field for any given sample, and α was determined without consideration of inhomogeneous linewidth broadening. It is therefore impossible to separate the LL damping and the inhomogeneous contributions to the measured linewidths. As such, these earlier studies in actuality provide only an upper limit for α. It is expected that the inhomogeneous linewidth contribution might well increase as the perpendicular anisotropy increases because the magnitude of the anisotropy variation would correspondingly increase. In fact, the inhomogeneous contribution to linewidth can exceed the LL contribution in perpendicularly oriented Co/Ni multilayers.[27,28]

It has also been reported that α, as determined from such single-frequency measurements, is proportional to anisotropy in Co/Pd and Co/Pt systems.[25,29] Such a proportionality is attributed to the fact that both anisotropy and intrinsic damping are indeed dependent on spin-orbit coupling.[25,29] However, the perpendicular anisotropy in multilayers also depends on the asymmetry of the orbital moment in a confined geometry.[30] As such, one should not necessarily expect anisotropy to be proportional to α for all sample systems, as we previously reported for the $Co_{90}Fe_{10}$/Ni system.[5]

To further clarify the relationship between anisotropy and α in multilayer systems, we systematically measured FMR spectra over a wide range of fields and frequencies for CoFe/Pd multilayer samples with varying thickness and CoFe:Pd thickness ratios. We separated the LL and inhomogeneous contributions to linewidth by standard methods to determine α. From these results, we were able to quantify the effect of spin pumping on the measured linewidths. We substitute $Co_{90}Fe_{10}$ (hereafter referred to as CoFe) for the more commonly used pure Co in order to suppress the face centered cubic (fcc)-to-hexagonal close packed (hcp) phase transition in thicker layers of Co, which simplifies our analysis.

II. EXPERIMENT

All samples were prepared at room temperature by dc magnetron sputter deposition at an Ar pressure of ∼0.07 Pa

TABLE I. Calculated and experimentally determined values of α for the CoFe/Pd multilayer samples.

CoFe:Pd Thickness ratio	t_{CoFe}^{ML} (nm)	t_{Pd}^{ML} (nm)	$\mu_0 M_{eff}$ (T)	t_{CoFe}^{eff} (nm)	α (experiment)	α (calculated)
1:3	0.5	1.5	−0.76	0.78	0.029 ± 0.002	0.044
	0.6	1.8	−0.44	0.88	0.038 ± 0.001	0.039
	0.7	2.1	−0.14	0.99	0.033 ± 0.002	0.036
	0.8	2.4	0.02	1.09	0.036 ± 0.002	0.033
1:2	0.35	0.7	−1.23	0.75	0.021 ± 0.007	0.044
	0.45	0.9	−0.78	0.85	0.022 ± 0.004	0.039
	0.5	1.0	−0.69	0.91	0.016 ± 0.002	0.037
	0.6	1.2	−0.31	1.00	0.028 ± 0.002	0.034
	0.8	1.6	0.08	1.22	0.028 ± 0.001	0.030
1:1	0.35	0.35	−0.59	1.13	0.017 ± 0.002	0.030
	0.45	0.45	−0.53	1.24	0.021 ± 0.003	0.028
	0.6	0.6	−0.13	1.40	0.017 ± 0.001	0.026
	0.8	0.8	0.23	1.60	0.018 ± 0.001	0.023
	1.0	1.0	0.46	1.81	0.017 ± 0.001	0.021

(0.5 mTorr). The base pressure of the chamber was $\approx 1 \times 10^{-7}$ Pa (1×10^{-9} Torr). Deposition rates were calibrated using x-ray reflectivity (XRR), which indicated a drift in deposition rates of less than 3% throughout the study. All samples consisted of a 3 nm Ta/3 nm Pd seed layer, which was previously shown to produce a highly (111)-textured microstructure with improved homogeneity of the magnetic anisotropy in Co/Pd multilayers.[31] Unless otherwise specified, a 3 nm Pd capping layer was also used to prevent oxidation.

We investigated three different series of samples of CoFe/Pd multilayers that had fixed CoFe-thickness (t_{CoFe}^{ML}) to Pd-thickness (t_{Pd}^{ML}) ratios of 1:1, 1:2, and 1:3. These multilayers were composed of 12 bilayers $[CoFe(t_{CoFe}^{ML})/Pd(t_{Pd}^{ML})] \times 12$ with a *total* multilayer thickness $t^{ML} = (t_{CoFe}^{ML} + t_{Pd}^{ML}) \times 12$. In order to investigate any influence of the anisotropy on linewidth, a thickness range for each sample series was chosen to provide a broad range of anisotropy values, ranging from out-of-plane to in-plane orientation. Since the perpendicular anisotropy is interfacial in origin, the anisotropy of the multilayer is straightforwardly varied by changing the thickness of the multilayer constituents. A list of the samples investigated is given in Table I.

The resonance field H_{res} and field-swept linewidth ΔH were measured using a broadband (1–60 GHz) perpendicular-geometry vector-network-analyzer ferromagnetic resonance (VNA-FMR) spectrometer.[32] The samples were placed face-down on a coplanar waveguide (CPW) with a 100-μm-wide center conductor. The microwave fields were applied to the sample by connecting port 1 of the VNA to the CPW. Port 2 of the VNA was then connected to the other end of the CPW, and the complex scattering parameter S_{21} was measured. Field-swept FMR spectra were obtained by measuring S_{21} at a fixed frequency f while the applied magnetic field was swept from high to low values. Figures 1(a) and 1(b) show real and imaginary components of exemplary spectra. The resonance field H_{res} and field-swept linewidth ΔH at each frequency f were determined by the fitting procedure outlined in Ref. 32. These fits are also included in Figs. 1(a) and 1(b).

In the perpendicular geometry employed here, the Kittel equation that describes the frequency-dependence of H_{res} is given by

$$H_{res}(f) = \frac{2\pi f}{|\gamma|\mu_0} + M_{eff}, \tag{1}$$

where $\gamma = (g\mu_B)/\hbar$ is the gyromagnetic ratio, g is the spectroscopic splitting factor, μ_B is the Bohr magneton, $\hbar$ is the reduced Planck's constant, μ_0 is the permeability of free space, M_{eff} is the effective magnetization defined by $M_{eff} = M_s - H_k$, M_s is the saturation magnetization, and H_k is the perpendicular anisotropy field. By this definition, positive and negative values of M_{eff} correspond to films with in-plane and out-of-plane orientations, respectively. Figure 1(c) shows an example of H_{res} as a function of f for a CoFe(0.6)/Pd(1.8) sample (thickness in nm). M_{eff} and g are determined by fitting the data to Eq. (1).

The frequency dependence of the field-swept linewidth ΔH was used to determine values of α and the inhomogeneous linewidth broadening ΔH_0 by fitting the data to[33–36]

$$\Delta H(f) = \frac{4\pi\alpha}{|\gamma|\mu_0} f + \Delta H_0. \tag{2}$$

An example of the linewidth data with fits to Eq. (2) is shown in Fig. 1(c). This equation shows that α is proportional to the slope of the data, whereas ΔH_0 is determined from the y-intercept. The two-magnon contribution to linewidth[37] was not accounted for in the fitting procedure because the perpendicular FMR geometry precludes the existence of degenerate spin-wave modes.[38]

For samples with the highest anisotropies (thinnest samples), it was necessary to perform measurements above 40 GHz in order to have the broad range of frequencies needed to obtain accurate measurements of α. While losses in the microwave circuit above 40 GHz were significantly larger, it was still possible to adequately fit the data for H_{res} and ΔH vs f, as shown in Fig. 2(a). However, we were unable to accurately extract ΔH for samples with small H_k (thicker samples) due to the presence of additional overlapping modes in the spectra, as shown in Fig. 2(b). Both the amplitude and overlap of the

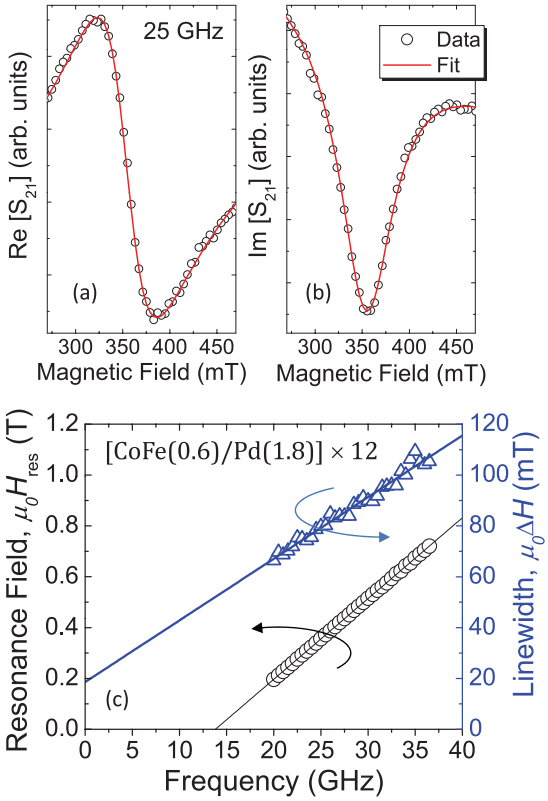

FIG. 1. (Color online) The (a) real and (b) imaginary FMR spectra for sample with CoFe:Pd = 1:3, (CoFe[0.6]/Pd[1.8]) × 12. Data were obtained from VNA measurements of the S_{21} scattering parameter at a fixed frequency of 25 GHz, as described in the body text. Fits of the spectra that used the LL equation are shown as solid red (dark gray) lines. (c) The resonance field H_{res} and field-swept linewidth ΔH as a function of frequency f for the same sample. Also shown as solid lines are fits to the data that were used to determine M_{eff}, α, and ΔH_0.

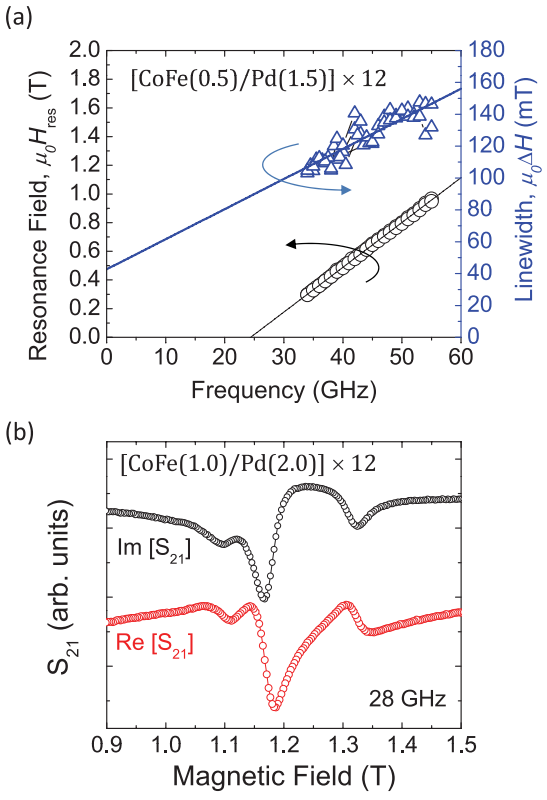

FIG. 2. (Color online) (a) The resonance field H_{res} and field-swept linewidth ΔH as a function of frequency f for a high-anisotropy sample (CoFe[0.5]/Pd[1.5] × 12). (b) The real and imaginary parts of S_{21} measured at f = 28 GHz for a thicker ML sample (CoFe[1.0]/Pd[2.0]) × 12. The spectra exhibit multiple overlapping modes that make it difficult to extract meaningful values for H_{res} and ΔH.

additional modes increased with increasing sample thickness. Fitting these data was further complicated by the fact that the three modes present in Fig. 2(b) have different phases relative to one another, which results in significant errors for the fitted linewidths. The origin of the additional modes is unknown. However, even with these limitations, we were able to measure FMR properties for samples with a range of almost 2 T for $\mu_0 H_k$.

III. RESULTS

A. FMR of CoFe/Pd multilayers

Figure 3(a) presents a plot of α vs M_{eff} for all three series of CoFe/Pd samples, where α varies over a range of 0.016 to 0.040. The data show little to no correlation of α with perpendicular anisotropy field. In contrast, a clear trend emerges when ΔH_0 is plotted vs M_{eff} [Fig. 3(b)]; ΔH_0 is initially negligible at positive values of M_{eff} (i.e., for in-plane anisotropy), but it then increases rapidly with increasingly negative M_{eff} (i.e., increasing H_k). This result is consistent with our previous findings for FMR with Co/Ni and CoFe/Ni multilayers, where we did not find any correlation between M_{eff} and α, but we did find a significant enhancement of ΔH_0 with increasing H_k.[5,27] The present data show that inhomogeneous broadening is a major contributing factor to the measured linewidth for this sample system.

A factor of great importance is the implication that inhomogeneous broadening cannot be neglected when extracting α from magnetization dynamics measurements in perpendicular-oriented multilayer materials. As further evidence for this implication, we have previously shown that ΔH_0 can be related to the spatial distribution of H_k in perpendicular Co/Ni multilayers where inhomogeneity was intentionally introduced via surface roughness.[27] It has been shown that perpendicularly magnetized multilayers exhibit significant anisotropy distributions.[39–41] Such distributions can result from variation of the microstructure, roughness, and interface across the material, for example. However, we have previously shown that the roughness of the multilayer increases with increasing thickness.[27,31] Since within each sample series, an increase in thickness results in an increase in M_{eff} (i.e., lower perpendicular anisotropy), the roughness cannot explain the trend in ΔH_0. It is possible that a large spatial variation of the intrinsic anisotropy can result in a substantial enhancement of inhomogeneous linewidth broadening with increasing anisotropy.

We will now concentrate on α and the experimental parameters that contribute to the large variation in α. The

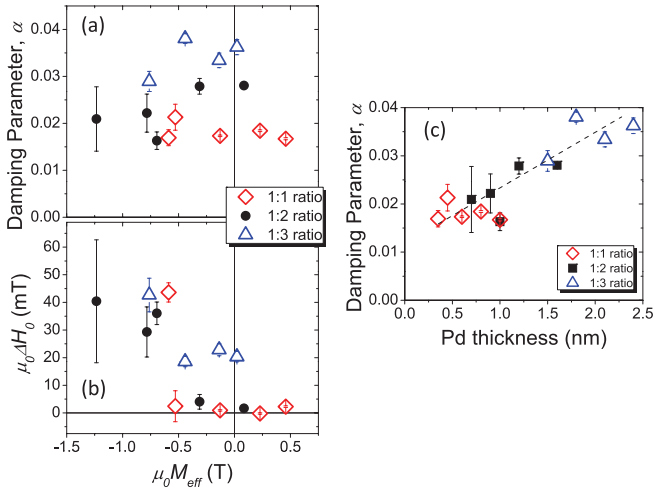

FIG. 3. (Color online) Extracted values for (a) α and (b) ΔH_0 as a function of M_{eff} for the ML samples. (c) The same data for α, but plotted as a function of Pd thickness $t_{\text{Pd}}^{\text{ML}}$. The dashed line is included as a guide to the eye.

damping parameter α is plotted as a function of $t_{\text{Pd}}^{\text{ML}}$ in Fig. 3(c). There is a clear trend that α increases with increasing $t_{\text{Pd}}^{\text{ML}}$. A likely explanation for these data is that α is enhanced in CoFe/Pd by spin pumping from the CoFe layers into the Pd layers.

To test the hypothesis that spin pumping is the most important source of enhanced damping, we will examine the various channels by which spin pumping can enhance α in the context of a complete multilayer (ML) structure, i.e., the ways in which the various spin-pumping processes between *all* the different layers contribute to the average damping of the total ML structure. Since consideration of the complete ML structure is particularly complicated given that there are many layers to account for in the full stack, we will first consider a structure that contains a single CoFe layer, and then we will systematically add additional layers to the system to gradually increase the complexity of the ML structure. This approach allows us to systematically evaluate the contribution of the different layers in the system to the overall damping.

B. Damping and spin pumping for ML structures with a single CoFe film

We deposited a series of ML structures with a single CoFe layer of thickness t_{CoFe} grown on a 3 nm Ta/3 nm Pd seed layer and capped with a 3 nm Pd layer (Fig. 4, inset). We found that the effective magnetization M_{eff} follows a linear $1/t_{\text{CoFe}}$ dependence, as shown in Fig. 4. Such dependence is indicative of both significant interface anisotropy and a consistent sample-to-sample quality. From the slope of the linear fit to the data in Fig. 4, we calculate the interface anisotropy energy density $K_s = (5.8 \pm 0.4) \times 10^{-4}$ J/m^2, which is in good agreement with previously reported values for Co/Pd.[10,31] Contributions from higher-order anisotropy terms have not been included in this calculation. The y-axis intercept yields a value of $\mu_0 M_s^{\text{CoFe}} = 1.80 \pm 0.01$ T for the bulk saturation magnetization of $Co_{90}Fe_{10}$. This value is within error bars of the value obtained from a stoichiometrically weighted average

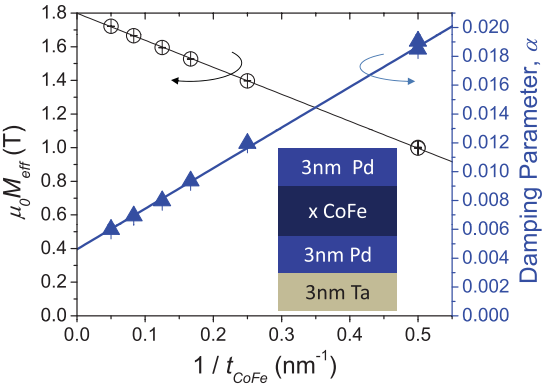

FIG. 4. (Color online) M_{eff} and α as a function of $1/t_{\text{CoFe}}$ for ML structures with a single CoFe layer and a fixed Pd-capping-layer thickness of 3 nm. The inset shows a schematic of the sample structure.

of the room-temperature saturation magnetizations of Fe and Co, and therefore the *bulk* higher-order anisotropy terms can be neglected in our analysis.

We also display α as a function of $1/t_{\text{CoFe}}$ in Fig. 4. The linear dependence of α on $1/t_{\text{CoFe}}$ suggests a significant interfacial contribution to the damping, as one would expect in the case of spin pumping.[15]

An important parameter for spin pumping is the real part of the spin-mixing conductance, $g^{\uparrow\downarrow}$. This parameter is proportional to the flux of angular momentum in the form of spin-polarized carriers that flow through the ferromagnet/nonmagnet interface in response to gyromagnetic precession in the ferromagnet. The enhanced damping that results from spin pumping into both the seed and capping layers for the single CoFe layer is predicted to have the following dependence with t_{CoFe}:[22]

$$\Delta\alpha_{\text{sp}}(t_{\text{CoFe}}) = g\mu_B \frac{g_{\text{eff}}^{\uparrow\downarrow}}{4\pi M_s} \frac{1}{t_{\text{CoFe}}}, \tag{3}$$

where $g_{\text{eff}}^{\uparrow\downarrow}$ is the real part of the *effective* spin-mixing conductance in units of m^{-2}. (The *effective* spin-mixing conductance accounts for the back flow of spin angular momentum from the nonmagnet back into the ferromagnet for both interfaces of the CoFe layer.) In the specific case of the single CoFe layer structures, the total LL damping of the system is

$$\alpha = \alpha_{\text{CoFe}} + \Delta\alpha_{\text{sp}}(t_{\text{CoFe}}). \tag{4}$$

Eq. (3) and Eq. (4) predict a linear dependence of α on $1/t_{\text{CoFe}}$, which is consistent with the data in Fig. 4. A linear regression fit to the data in Fig. 4 yields $\alpha_{\text{CoFe}} = 0.00462 \pm 0.00004$ for the LL damping in bulk $Co_{90}Fe_{10}$, and $g_{\text{eff}}^{\uparrow\downarrow} = (2.48 \pm 0.04) \times 10^{19}$ m^{-2}.

In order to model the total spin-pumping contribution to LL damping in ML structures, we require the *intrinsic* spin-mixing conductance $g^{\uparrow\downarrow}$ of a single CoFe/Pd interface. This value cannot be obtained from the data in Fig. 4, since the individual contributions from the seed and capping layers cannot be separated. In addition, we require the spin-diffusion length for Pd, λ_{Pd}, because the depolarization of pumped spins in the Pd layer depends on the thickness of the Pd layer relative to λ_{Pd}. In other words, the thicker the Pd layer, the more likely

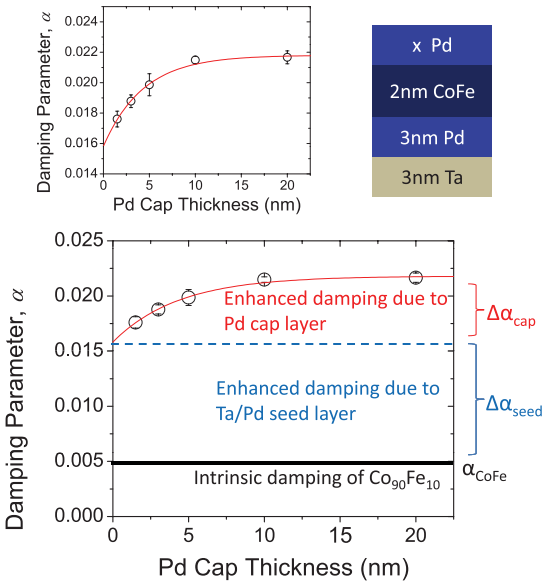

FIG. 5. (Color online) The damping parameter α for ML structures with a single CoFe layer and a fixed CoFe-layer thickness of 2 nm, plotted as a function of Pd-capping-layer thickness. The plot includes a fit of the data to Eq. (5)–(7) (solid red/dark gray line). To the right of the figure, we indicate the relative contributions to α by spin pumping at the top CoFe/Pd interface, bottom CoFe/Pd interface, and the intrinsic, bulk-like damping of the CoFe layer itself. A schematic of the sample structure and a magnified view of the data over a narrower range of damping values are included at the top.

it is that a spin-flip scattering event will occur before a spin returns to the CoFe/Pd interface. To determine $\lambda_{\rm Pd}$ and $g_{\rm Pd}^{\uparrow\downarrow}$ for the CoFe/Pd interface, we deposited a series of samples with a constant CoFe layer thickness of 2 nm and a varied Pd capping-layer thickness $t_{\rm Pd}$, as shown schematically in Fig. 5. We show in Fig. 5 the dependence of α on $t_{\rm Pd}$. The enhanced damping due to spin pumping is now described by[42]

$$\Delta\alpha_{\rm Pd}^{\rm cap} = g\mu_B \frac{g_{\rm Pd}^{\uparrow\downarrow}}{4\pi M_s} \frac{1}{t_{\rm CoFe}} (1 - e^{\frac{-2t_{\rm Pd}}{\lambda_{\rm Pd}}}). \quad (5)$$

The additional bracketed term on the right accounts for the return of spins to the CoFe/Pd interface; the fraction of pumped spin current that manages to reflect from the Pd/air interface and return to the ferromagnet adds angular momentum (previously lost) to the ferromagnet, thereby reducing the *effective* spin-mixing conductance. The factor of 2 in the exponent assumes that the Pd/air interface is a perfect reflector of spin. (Spins that reflect from the Pd/air interface must traverse a total distance that is twice the thickness of the Pd layer before returning angular momentum to the CoFe layer.) We define the *effective* spin-mixing conductance of the Pd capping layer as

$$g_{\rm eff\_Pd}^{\uparrow\downarrow}(t_{\rm Pd}) = g_{\rm Pd}^{\uparrow\downarrow}(1 - e^{\frac{-2t_{\rm Pd}}{\lambda_{\rm Pd}}}). \quad (6)$$

The total *effective* spin-mixing conductance of the single CoFe layer structure is given by

$$g_{\rm eff}^{\uparrow\downarrow} = g_{\rm eff\_seed}^{\uparrow\downarrow} + g_{\rm eff\_Pd}^{\uparrow\downarrow}(t_{\rm Pd}). \quad (7)$$

The data in Fig. 5 show an exponential dependence of α on $t_{\rm Pd}$, with an asymptotic value of $\alpha = 0.0218 \pm 0.0002$ as $t_{\rm Pd}^{\rm cap} \to \infty$ and an intercept value of $\alpha = 0.0158 \pm 0.0005$ at $t_{\rm Pd}^{\rm cap} = 0$. The enhanced damping at $t_{\rm Pd} = 0$ is due solely to spin pumping into the seed layer, whereas the continuous increase in α with increasing $t_{\rm Pd}$ is due to spin pumping in the Pd cap. As seen in Fig. 5, the seed layer enhances α by $\Delta\alpha_{\rm seed}$ relative to the bulk CoFe value of $\alpha_{\rm CoFe} = 0.0046$ that was determined previously. The asymptotic value at $t_{\rm Pd}^{\rm cap} \to \infty$ can then be used to determine $g_{\rm Pd}^{\uparrow\downarrow}$ once $\Delta\alpha_{\rm seed}$ is accounted for.

A fit is included in Fig. 5 with $g_{\rm Pd}^{\uparrow\downarrow}$, $g_{\rm eff_{seed}}^{\uparrow\downarrow}$, and $\lambda_{\rm Pd}$ as the fitting parameters. The fit yields values of $g_{\rm Pd}^{\uparrow\downarrow} = (1.07 \pm 0.13) \times 10^{19}$ m^{-2}, $g_{\rm eff_{seed}}^{\uparrow\downarrow} = (2.01 \pm 0.10) \times 10^{19}$ m^{-2}, and $\lambda_{\rm Pd} = (8.6 \pm 1.0)$ nm. The fitted spin-diffusion length is within error bars of a previously reported room-temperature value of 9 nm[42] that was obtained in a similar manner as discussed here. Similarly, the fitted value for $g_{\rm Pd}^{\uparrow\downarrow}$ is very close to the previously reported value of 0.9×10^{19} m^{-2} from the same study.[42] It is interesting to point out that the measurements in Ref. 42 were performed using an in-plane geometry. Thus, the spin-pumping process is largely unaffected by the direction of magnetization.

C. Spin-pumping effects in ML structures with two CoFe layers

We showed in the previous section that the spin-pumping mechanism provides an adequate explanation for the dependence of damping on Pd capping-layer thickness in a sample system with a single CoFe layer. We now present results for a ML sample system where a Pd layer is inserted between two $Co_{90}Fe_{10}$ layers. Such a sample allows us to examine how spin pumping affects damping when a spin current generated by one CoFe layer interacts with a second CoFe layer. A schematic of this structure presented in Fig. 6(a). For this sample system, we deposited a variable-thickness Pd layer of thickness $t_{\rm Pd}^{\rm int}$ (hereafter referred to as the Pd *interlayer*) in the center of a 2-nm-thick CoFe layer, effectively dividing the CoFe layer into two 1-nm-thick layers.

We show the dependence of α on $t_{\rm Pd}^{\rm int}$ in Fig. 6(b). The damping is rapidly enhanced as $t_{\rm Pd}^{\rm int}$ increases from 0 to 3 nm. The horizontal lines included in Fig. 6(b) indicate the values of α for the ML structures with a single 1- and 2-nm-thick CoFe layer. (The value of α for a single 1-nm-thick CoFe layer was obtained by interpolation of the data in Fig. 4.) Over the range of $t_{\rm Pd}^{\rm int} = 0$–3 nm, the damping is seen to linearly increase from the expected value for a ML with a single 2 nm CoFe layer to that of a 1 nm CoFe layer. For $t_{\rm Pd}^{\rm int} > 3$ nm, α continues to increase with increasing $t_{\rm Pd}^{\rm int}$, albeit at a much more gradual rate.

The data in Fig. 6(b) appear to suggest that the primary role of the intermediate Pd layer with regard to damping is to simply decouple the two 1-nm-thick CoFe layers from each other, such that, in the limit of an infinitely thick intermediate Pd layer, the spins pumped into the cap and seed layers are only drawn from the respective spin reservoirs formed by the individual 1-nm-thick CoFe layers adjacent to the cap and seed layers. A striking feature of this decoupling is the manner in which the damping associated with spin pumping at each interface simply adds together to yield the net damping of the total ML structure. In other words, the decoupling does not result in two degenerate resonances, each with a different

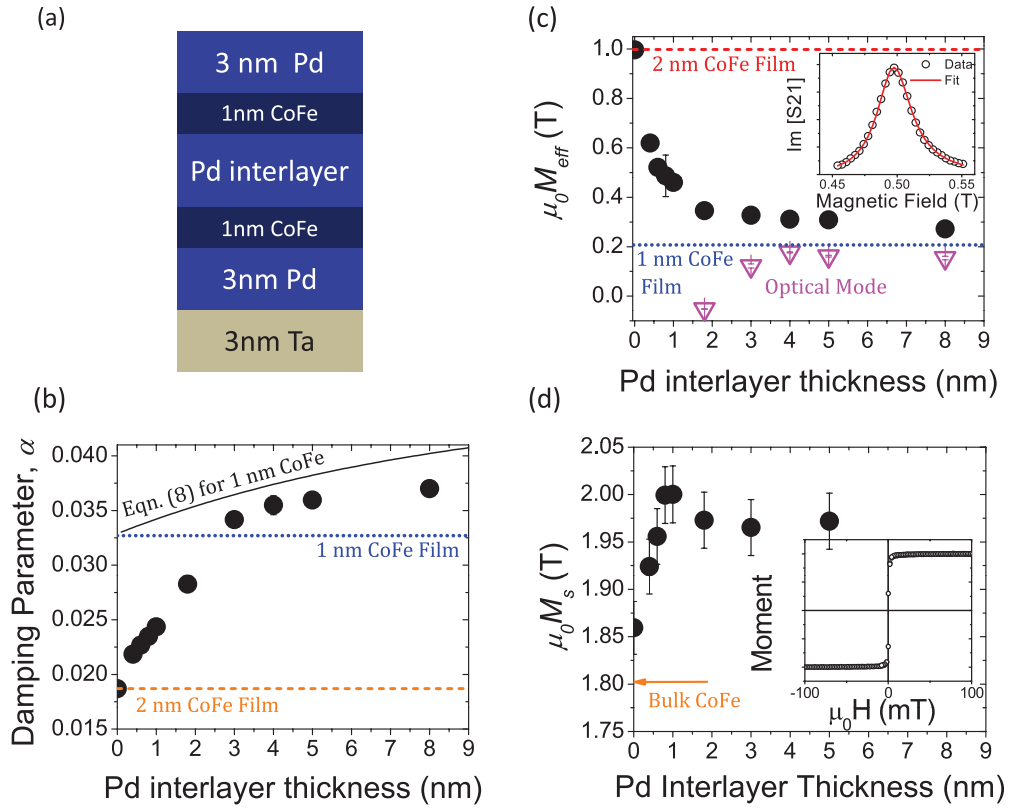

FIG. 6. (Color online) (a) Schematics of the sample structure of the ML structures with only two CoFe layers separated by a Pd interlayer. (b) Plot of α as a function of Pd interlayer thickness $t_{\mathrm{Pd}}^{\mathrm{int}}$. The lower horizontal line corresponds to the measured value of α shown in Fig. 4 for a ML with a single 2-nm-thick CoFe layer. The upper horizontal line is extrapolated from the data in Fig. 4 for the unmeasured case of a ML with a single 1-nm-thick CoFe layer. The solid line is the theoretically predicted values of α by use of Eq. (8) for a 1 nm CoFe layer. (c) Plots of M_{eff} and (d) M_s vs increasing Pd interlayer thickness. The inset in (c) is the 7 GHz spectrum of the FMR mode and fit for the $t_{\mathrm{Pd}}^{\mathrm{int}} = 8$ nm sample. The inset in (d) is an example of SQUID hysteresis data that were used to determine M_s.

linewidth as a result of the different spin-pumping–induced damping in each layer. Instead, the two CoFe layers appear to be decoupled with regard to the spin-pumping mechanism but still coupled with regard to the net damping process.

To gain further insight into the dependence of α on $t_{\mathrm{Pd}}^{\mathrm{int}}$, we consider the dependence of M_{eff} on $t_{\mathrm{Pd}}^{\mathrm{int}}$, which is shown in Fig. 6(c) as the filled black circles. As is the case for the damping data in Fig. 6(b), the expected values of M_{eff} for individual 2-nm- and 1-nm-thick CoFe layers (determined from Fig. 4) are indicated with horizontal lines. Over the range of $t_{\mathrm{Pd}}^{\mathrm{int}} = 0$–3 nm, M_{eff} decreases rapidly with increasing $t_{\mathrm{Pd}}^{\mathrm{int}}$, such that M_{eff} approaches the value observed for the 1-nm-thick CoFe layer in the structures with a single CoFe layer in the limit of infinite intermediate-Pd-layer thickness. One explanation of this effect is that the electronic orbital states that drive the interfacial anisotropy depend strongly on the separation of the CoFe layers by Pd for intermediate layers up to ~3 nm thick.[43,44] Alternatively, this decrease in M_{eff} could result from the decreasing coupling between the layers as they progressively become independent 1-nm-thick layers at large values of $t_{\mathrm{Pd}}^{\mathrm{int}}$.

Evidence for a longer range magnetic coupling between the two layers is apparent in the weaker FMR spectral peak at lower applied fields. We attribute this peak to an optical mode for the two CoFe layers, whereby the two layers precess with a 180 degree phase difference. The angular misalignment of the two layers results in an additional exchange field H_{ex} acting on each layer. Under such circumstances, the spectroscopic effective magnetization for the optical mode $M_{\mathrm{eff}}^{\mathrm{opt}}$ is given by $M_{\mathrm{eff}}^{\mathrm{opt}} = M_s - H_k - H_{\mathrm{ex}}$. The splitting between the optical mode (magenta triangles in Fig. 6) and acoustic FMR modes is a measure of the exchange field that couples the two layers. We see from the data in Fig. 6(c) that the interlayer coupling falls off rapidly with increasing Pd thickness for $t_{\mathrm{Pd}}^{\mathrm{int}} < 4$ nm, but then persists with a much slower rate of reduction for $t_{\mathrm{Pd}}^{\mathrm{int}} > 4$ nm. Even at $t_{\mathrm{Pd}}^{\mathrm{int}} = 8$ nm, 0.1 T of splitting remains between the optical and acoustic FMR modes. The coupling between the CoFe layers prevents them from precessing independently, as evidenced by a single spectral peak for the acoustic FMR mode that is well fitted by the LL equation for a single mode, an example of which is presented as an inset in Fig. 6(c) ($f = 7$ GHz, $t_{\mathrm{Pd}}^{\mathrm{int}} = 8$ nm). (The existence of two independent nondegenerate modes or two independent degenerate modes with unequal linewidths would show a deviation from the LL equation fit. It is unlikely that two independent degenerate modes would have equal values of linewidth since the effective spin-mixing conductance values of the top and bottom layers are different.)

We also performed superconducting quantum interference device (SQUID) magnetometry on the same samples to

measure the saturation magnetization M_s, which is shown in Fig. 6(d). An applied field of $\mu_0 H = 100$ mT was sufficient to fully saturate the magnetization, as shown in the inset in Fig. 6(d). M_s was determined by normalization of the measured moment by the nominal volume of CoFe. The bulk spectroscopic value of $\mu_0 M_s = 1.80$ T, as determined by extrapolation of the FMR data in Fig. 4, is also indicated in the figure. All measured values of M_s for the ML structures are greater than the spectroscopic bulk value. M_s initially increases with increasing $t_{\mathrm{Pd}}^{\mathrm{int}}$ until it peaks at 1 nm. The magnetization then drops slightly with increasing intermediate-Pd-layer thickness until it saturates for $t_{\mathrm{Pd}}^{\mathrm{int}} > 3$ nm. We interpret the enhancement of M_s relative to the spectroscopic bulk value to be a result of the partial polarization of Pd atoms that are within a few nanometers of CoFe, consistent with theoretical predictions and previous experimental results.[31,43–45] In other words, the first few nanometers of Pd in contact with CoFe are magnetic, therefore mediating exchange-coupling between the two CoFe layers. In fact, exchange coupling through several nanometers of Pd in Fe/Pd ML structures was previously reported.[46–49] Such exchange coupling would partially explain the transition of α from a value measured with a single 2-nm-thick CoFe layer to a value equal to that of a single 1-nm-thick layer; as the exchange coupling between the CoFe layers is reduced with increasing $t_{\mathrm{Pd}}^{\mathrm{int}}$, the magnetic layers increasingly behave as isolated layers.

It is clear from the data in Figs. 6(c) and 6(d) that, in fact, two distinct mechanisms couple the two CoFe layers through the intermediate Pd layer. A shorter-range mechanism correlates the presumptive spin polarization induced in the Pd due to proximity to the CoFe layer. Such a mechanism is reminiscent of the direct exchange that can exist between two proximate ferromagnetic layers, as in exchange spring structures.[50] However, a longer-range coupling mechanism appears to extend far beyond the 2 nm range of the proximity-induced polarization in Pd. Given the measured spin diffusion length of $\lambda_{\mathrm{Pd}} \approx 9$ nm for Pd, we conclude that the longer-range coupling is facilitated by the so-called dynamic exchange interaction, whereby the spin current generated by spin pumping in one ferromagnetic layer is then absorbed by a second ferromagnetic layer separated from the first by a nonmagnetic spacer layer.[16] As long as the spacer layer thickness is less than the spin diffusion length, the dynamic exchange mechanism can effectively couple the precessional dynamics of two magnetic layers, causing the two layers to exhibit identical values for the linewidth in the event that the resonance fields for the layers are degenerate.[51]

Returning to the data in Fig. 6(b), we see that α for samples with $t_{\mathrm{Pd}}^{\mathrm{int}} > 3$ nm is enhanced above that predicted for an individual 1-nm-thick CoFe layer. In the context of the previous interpretation of the damping enhancement as a result of spin pumping, these data indicate that spin pumping into the Pd interlayer also contributes to the net damping. Thus, in the limit of large-Pd-interlayer thickness, the net damping for the ML with two 1-nm-thick CoFe layers behaves as though it were a single 1-nm-thick CoFe layer (by virtue of the dynamic exchange coupling) with spin pumping into a 3 nm Pd cap, a Pd/Ta seed layer with 3 nm of Pd and 3 nm of Ta, and a third damping channel associated with spin pumping into the Pd interlayer. We assume that the spin current originating in one of the CoFe layers via spin pumping is reabsorbed by the other layer, partially compensating for the loss of spin that results in enhanced damping. If we use an effective spin-mixing conductance for the entire ML given by

$$g_{\mathrm{eff\_ML}}^{\uparrow\downarrow} = g_{\mathrm{eff\_seed}}^{\uparrow\downarrow} + g_{\mathrm{eff\_Pd}}^{\uparrow\downarrow}(t_{\mathrm{Pd}} = 3\mathrm{nm}) + g_{\mathrm{Pd}}^{\uparrow\downarrow}\left(1 - e^{\frac{-t_{\mathrm{Pd}}^{\mathrm{int}}}{\lambda_{\mathrm{Pd}}}}\right), \quad (8)$$

the additional enhancement due to the Pd interlayer can be described. (Note that the factor of 2 is no longer present in the exponent since the pumped spins are assumed to travel directly from one CoFe layer to the other CoFe layer, and therefore, the pumped spins travel only a distance of $t_{\mathrm{Pd}}^{\mathrm{int}}$ in the Pd.) Equation 8 is plotted in Fig. 6(b) as the solid black curve using a value of $t_{\mathrm{CoFe}} = 1$ nm. While this equation overestimates values for α, the experimental data are seen to approach this curve at larger values of $t_{\mathrm{Pd}}^{\mathrm{int}}$.

We can further improve upon this model by consideration of the value of t_{CoFe} used in the calculation of α. Both M_{eff} and α show a smooth transition from the expected behavior of a 2 nm CoFe film to that of a 1 nm CoFe film as the Pd interlayer thickness is increased. In other words, upon insertion of the Pd interlayer in the middle of the 2 nm CoFe layer, the magnetic properties do not immediately resemble two isolated 1 nm CoFe layers. In fact, the system behaves as if the thickness of the CoFe layer is steadily reduced over several nanometers of $t_{\mathrm{Pd}}^{\mathrm{int}}$.

We therefore introduce an *effective* thickness $t_{\mathrm{CoFe}}^{\mathrm{eff}}$ of the CoFe layer. Since the two CoFe layers are exchange coupled to some degree, a particular CoFe layer has a larger spin bath available to it than the number of spins contained within the layer itself. As a result, despite the 1 nm physical thickness of the CoFe layers, the *effective* volumes of the CoFe layers are enhanced as a result of the availability of additional spins. We assume that the available spins are a function of the Pd interlayer thickness that decreases as $t_{\mathrm{Pd}}^{\mathrm{int}}$ increases (i.e., as the exchange interaction decreases). Thus, we define the effective thickness as $t_{\mathrm{CoFe}}^{\mathrm{eff}}(t_{\mathrm{CoFe}}, t_{\mathrm{Pd}}^{\mathrm{int}}) = t_{\mathrm{CoFe}} + \varepsilon(t_{\mathrm{Pd}}^{\mathrm{int}})\, t_{\mathrm{CoFe}}$, where $\varepsilon(t_{\mathrm{Pd}}^{\mathrm{int}})$ is the effective coupling between the layers (see supplementary material for details[52]). If we assume that $\varepsilon(t_{\mathrm{Pd}}^{\mathrm{int}})$ is the same for the anisotropy and damping process, then we can generate approximate values of $t_{\mathrm{CoFe}}^{\mathrm{eff}}$ from the data in Fig. 6(c) by applying the relationship extracted between M_{eff} and t_{CoFe} in Fig. 4.

Figure 7(a) is a plot of the values determined for $t_{\mathrm{CoFe}}^{\mathrm{eff}}$ as a function of $t_{\mathrm{Pd}}^{\mathrm{int}}$. Values of α calculated using the effective thickness and the effective spin mixing conductance given in Eq. (8) are plotted in Fig. 6(b) as the red open triangles. Below $t_{\mathrm{Pd}}^{\mathrm{int}} = 2$ nm, the model reasonably describes the experimental data despite the fact that it still overestimates α. However, above $t_{\mathrm{Pd}}^{\mathrm{int}} = 2$ nm, the model is in good quantitative agreement with the data. The deviation of the model from the data at $t_{\mathrm{Pd}}^{\mathrm{int}} \leqslant 2$ nm is not surprising when considering the complex (and not fully understood) coupling between the layers, as well as the influence of the polarized region within the Pd layer, which cannot be fully accounted for in the model. In other words, the assumption that $\varepsilon(t_{\mathrm{Pd}}^{\mathrm{int}})$ is the same for the anisotropy and damping process may not strictly hold within the first few nanometers of Pd.

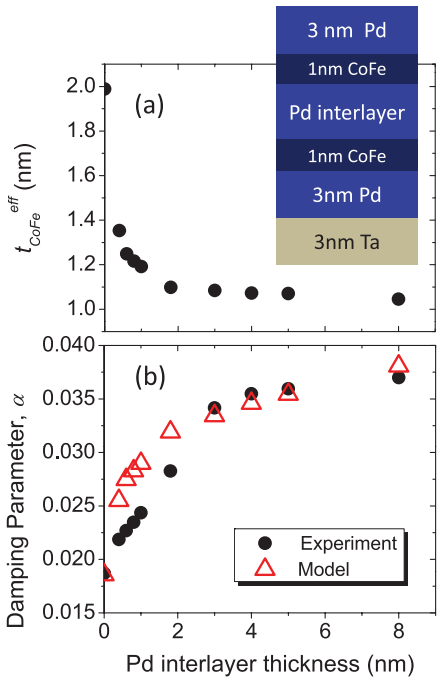

FIG. 7. (Color online) A plot of (a) the effective thickness $t_{\mathrm{CoFe}}^{\mathrm{eff}}$ and (b) α as a function of the Pd interlayer thickness. The open triangles are the predicted values of α obtained with the model using $t_{\mathrm{CoFe}}^{\mathrm{eff}}$.

IV. DISCUSSION

The data presented in Fig. 5 along with the fitting result showing $g_{\mathrm{eff}_{\mathrm{seed}}}^{\uparrow\downarrow} \approx 2\, g_{\mathrm{Pd}}^{\uparrow\downarrow}$ warrant additional discussion. Even if the Pd/Ta interface were to act as a perfect spin sink, which depolarizes all of the incident spin current, an incorrect interpretation of Eq. (6) would lead us to expect $g_{\mathrm{eff}_{\mathrm{seed}}}^{\uparrow\downarrow} \leqslant g_{\mathrm{Pd}}^{\uparrow\downarrow}$, based on the fact that the flux of spins being pumped into the top and bottom Pd layers would be identical and cannot exceed $g_{\mathrm{Pd}}^{\uparrow\downarrow}$. This interpretation is in contrast to the experimental data presented in Fig. 5, which shows $g_{\mathrm{eff}_{\mathrm{seed}}}^{\uparrow\downarrow} > g_{\mathrm{Pd}}^{\uparrow\downarrow}$. The differing values for $g_{\mathrm{eff}_{\mathrm{seed}}}^{\uparrow\downarrow}$ and $g_{\mathrm{Pd}}^{\uparrow\downarrow}$ can be reasonably explained if one assumes that the spin current is diffusive in the Pd layer;[22] any given spin that is pumped from the CoFe layer into an infinitely thick Pd layer has a finite probability of diffusing back to the CoFe/Pd interface before a spin-flip event depolarizes the spin in the Pd layer. In the limit of purely diffusive spin transport and a large ratio of the spin diffusion length (spin-flip scattering) to spin mean free path (spin-conserving scattering), it can be shown by a straightforward one-dimensional calculation that there is an ~61% probability for a spin to diffuse back to the magnetic layer before depolarizing (see supplementary material[53]). As such, the fitted value for $g_{\mathrm{Pd}}^{\uparrow\downarrow}$ by use of Eq. (5) and Eq. (6) is in actuality ~2.6× smaller than the true, intrinsic spin-mixing conductance associated with the CoFe/Pd interface because the damping is enhanced by only 39% of the maximum possible amount. On the other hand, in the limit of an infinitesimally thin Pd layer bounded by a perfect spin sink, the probability reduces to zero for a spin to diffuse back to the CoFe/Pd interface before a spin-flip scattering event, and the resultant enhancement of damping would be maximal. This would explain the approximate 2× difference between the fitted values for $g_{\mathrm{eff}_{\mathrm{seed}}}^{\uparrow\downarrow}$ and $g_{\mathrm{Pd}}^{\uparrow\downarrow}$, assuming that the Pd/Ta interface is indeed a strong spin sink and the Pd layer thickness is comparable to or less than the spin mean free path. Previously reported data indicate that 5-nm-thick Ta is indeed an effective spin sink.[23]

It has been argued that spin-diffusion theory is not applicable for Pd films thinner than the electronic-momentum mean free path, estimated to be in excess of 9 nm.[42] However, the evidence for proximity-induced magnetization in Pd suggests that there is a significant degree of exchange overlap between the carriers in Pd. Such exchange coupling, even if insufficient to sustain ferromagnetic order at finite temperature, is presumably an effective mechanism for the propagation and diffusion of spin in conductors. If exchange is the dominant mechanism for spin diffusion in Pd, as opposed to diffusion of spin-polarized carriers, one would expect an extremely short spin mean free path, though in this case, the scattering events that transfer spin from one carrier to another via exchange would still conserve angular momentum. This is in contrast to scattering processes that do not conserve spin, such as the spin-paramagnon scattering process postulated in Ref. 42. As such, we conjecture that the spin mean free path is much shorter than the spin diffusion length in Pd, where the former refers to a spin-conserving scattering process, and the latter refers to a non-spin-conserving scattering process.

The reasonable agreement between the data and model presented in Fig. 7(b) indicates that spin pumping is sufficient to explain the dominant contribution to the enhanced damping observed in the Pd/CoFe/Pd/CoFe/Pd system. The natural next step is to apply this model to full CoFe/Pd multilayer systems. In this case, we follow the same procedure used in modeling the Pd/CoFe/Pd/CoFe/Pd system, but instead insert 11 Pd interlayers into a CoFe layer that has a total thickness of $12 \times t_{\mathrm{CoFe}}^{\mathrm{ML}}$. This model produces a multilayer structure with 12 bilayers that is comparable to the samples that were experimentally measured. By using the same proportionality relationship between t_{Pd} and $t_{\mathrm{CoFe}}^{\mathrm{eff}}$ determined in Fig. 7(a), the effective thickness of t_{CoFe} in the multilayers was approximated and is reported in Table I for the ML samples measured in this study. The values of α calculated using the effective thickness and Eq. (8) are also reported in Table I, along with the experimentally determined values of α. Reasonable quantitative agreement is found between the calculated and experimentally determined values of α when $t_{\mathrm{CoFe}}^{\mathrm{ML}} > 0.5$ nm. For values of $t_{\mathrm{CoFe}}^{\mathrm{ML}} \leqslant 0.5$ nm (shaded data in Table I), the model overestimates α.

The disagreement of the model for $t_{\mathrm{CoFe}}^{\mathrm{ML}} \leqslant 0.5$ nm is not surprising considering that a monolayer of CoFe is approximately 0.3 nm. Thus, at $t_{\mathrm{CoFe}}^{\mathrm{ML}} = 0.5$ nm, the coverage of CoFe is less than 2 monolayers. From a spin-pumping perspective, a Co or Fe atom that is in contact with both interfaces (as is the case for a single monolayer) will be performing "double duty," and it is reasonable to assume that the pumped spin currents into either interface would be reduced relative to the situation where Co or Fe atoms are in contact with only one interface. Thus, we speculate that the spin-pumping contribution to the damping would be reduced as the CoFe layer decreases below 2 monolayers. In addition,

the thickness range of the Pd is within that of the short-range interlayer exchange coupling displayed in the data in Fig. 6 ($t_{Pd}^{int} < 3$ nm). As such, we expect the dynamic exchange coupling between the layers to be nearly maximal. The effect of such exchange coupling in the spin-pumping or damping process is still not understood. This highlights the fact that, to our knowledge, there is an absence of a theoretical description of the exchange interaction and the effect that the polarized Pd has on the spin-pumping and damping process. Such a description would be invaluable to more accurately model the damping process in the full multilayer structures. Finally, we have thus far treated the interfaces as ideal transitions from one material to the other. It is certainly reasonable to expect some intermixing of the interfacial species. Such effects would be more pronounced as t_{CoFe}^{ML} is reduced to a single monolayer.

V. CONCLUSIONS

We systematically measured α in CoFe/Pd multilayers with varying thickness and CoFe:Pd thickness ratios using perpendicular geometry VNA-FMR. Of importance to technological applications, we find that α varies between 0.016 and 0.04 and that the large values of α previously reported were likely due to inhomogeneous broadening. We explicitly show that the inhomogeneous contribution to the linewidth cannot be ignored in the measurement of the damping parameter, which is especially true in samples with significant perpendicular anisotropy. In fact, our data show that the inhomogeneous contribution to the linewidth increases as the anisotropy increases. In contrast, we show that α is independent of anisotropy, but it depends instead on the thickness of the CoFe and Pd layers. We quantified the spin-pumping contribution to the enhanced damping of the system by taking the spin-diffusion length of Pd and the spin-mixing conductance of the CoFe-Pd interface into account. From the experimentally determined parameters of the spin-mixing conductance and spin-diffusion length of Pd, as well as an inferred effective magnetic volume that accounts for both static and dynamic exchange coupling between magnetic layers, we were able to quantitatively model the damping parameter in Pd/CoFe/Pd/CoFe/Pd multilayers. The model captures the essential qualitative observation that increased Pd spacing between the CoFe layers leads to enhanced damping. We conclude that spin pumping adequately describes the dominant source of enhanced damping in these materials.

ACKNOWLEDGMENTS

The authors are grateful to Mike Schneider for valuable discussions; Denis LeGolvan and Mitch Wallis for use of the 67 GHz VNA; and Tom Cecil, Bill Rippard, Tony Kos, and Steve Russek for assistance with the deposition chamber.

*justin.shaw@nist.gov

[1] S. Mangin, D. Ravelosona, J. A. Katine, M. J. Carey, B. D. Terris, and E. E. Fullerton, Nat. Mater. **5**, 210 (2006).
[2] W. H. Rippard, A. M. Deac, M. R. Pufall, J. M. Shaw, M. W. Keller, S. E. Russek, G. E. W. Bauer, and C. Serpico, Phys. Rev. B **81**, 014426 (2010).
[3] B. D. Terris and T. Thomson, J. Phys. D **38**, R199 (2005).
[4] G. H. O. Daalderop, P. J. Kelly, and F. J. A. den Broeder, Phys. Rev. Lett. **68**, 682 (1992).
[5] J. M. Shaw, H. T. Nembach, and T. J. Silva, Appl. Phys. Lett. **99**, 012503 (2011).
[6] S. Hashimoto, Y. Ochiai, and K. Aso, J. Appl. Phys. **66**, 4909 (1989).
[7] T. Suzuki, H. Notarys, D. C. Dobbertin, C.-J. Lin, D. Weller, D. C. Miller, and G. Gorman, IEEE Trans. Magn. **28**, 2754 (1992).
[8] W. B. Zeper, H. W. Vankesteren, B. A. J. Jacobs, J. H. M. Spruit, and P. F. Carcia, J. Appl. Phys. **70**, 2264 (1991).
[9] R. L. Stamps, L. Louail, M. Hehn, M. Gester, and K. Ounadjela, J. Appl. Phys. **81**, 4751 (1997).
[10] B. N. Engel, C. D. England, R. A. VanLeeuwen, M. H. Wiedmann, and C. M. Falco, Phys. Rev. Lett. **67**, 1910 (1991).
[11] R. Law, R. Sbiaa, T. Liew, and T. C. Chong, Appl. Phys. Lett. **91**, 242504 (2007).
[12] S. Sindhu, M. A. M. Haast, K. Ramstöck, L. Abelmann, and J. C. Lodder, J. Magn. Magn. Mater. **238**, 246 (2002).
[13] S. Mangin, Y. Henry, D. Ravelosona, J. A. Katine, and E. E. Fullerton, Appl. Phys. Lett. **94**, 012502 (2009).
[14] R. Urban, G. Woltersdorf, and B. Heinrich, Phys. Rev. Lett. **87**, 217204 (2001).
[15] Y. Tserkovnyak, A. Brataas, and G. E. W. Bauer, Phys. Rev. Lett. **88**, 117601 (2002).
[16] B. Heinrich, Y. Tserkovnyak, G. Woltersdorf, A. Brataas, R. Urban, and G. E. W. Bauer, Phys. Rev. Lett. **90**, 187601 (2003).
[17] K. Lenz, T. Tolinski, J. Lindner, E. Kosubek, and K. Baberschke, Phys. Rev. B **69**, 144422 (2004).
[18] L. Lagae, R. Wirix-Speetjens, W. Eyckmans, S. Borghs, and J. De Boeck, J. Magn. Magn. Mater. **286**, 291 (2005).
[19] J.-M. L. Beaujour, J. H. Lee, A. D. Kent, K. Krycka, and C.-C. Kao, Phys. Rev. B **74**, 214405 (2006).
[20] H. Lee, L. Wen, M. Pathak, P. Janssen, P. LeClair, C. Alexander, C. K. A. Mewes, and T. Mewes, J. Phys. D: Appl. Phys. **41**, 215001 (2008).
[21] O. Mosendz, G. Woltersdorf, B. Kardasz, B. Heinrich, and C. H. Back, Phys. Rev. B **79**, 224412 (2009).
[22] O. Mosendz, V. Vlaminck, J. E. Pearson, F. Y. Fradin, G. E. W. Bauer, S. D. Bader, and A. Hoffmann, Phys. Rev. B **82**, 214403 (2010).
[23] T. Gerrits, M. L. Schneider, and T. J. Silva, J. Appl. Phys. **99**, 23901 (2006).
[24] A. Barman, S. Wang, O. Hellwig, A. Berger, E. E. Fullerton, and H. Schmidt, J. Appl. Phys. **101**, 09D102 (2007).
[25] S. Pal, B. Rana, O. Hellwig, T. Thomson, and A. Barman, Appl. Phys. Lett. **98**, 082501 (2011).
[26] N. Fujita, N. Inaba, F. Kirino, S. Igarashi, K. Koike, and H. Kato, J. Magn. Magn. Mater. **320**, 3019 (2008).
[27] J. M. Shaw, H. T. Nembach, and T. J. Silva, J. Appl. Phys. **108**, 093922 (2010).
[28] T. Kato, Y. Matsumoto, S. Okamoto, N. Kikuchi, O. Kitakami, N. Nishizawa, S. Tsunashima, S. Iwata, IEEE Trans. Magn. **47**, 3036 (2011).

[29]S. Mizukami, E. P. Sajitha, D. Watanabe, F. Wu, T. Miyazaki, H. Naganuma, M. Oogane, and Y. Ando, Appl. Phys. Lett. **96**, 152502 (2010).
[30]D. Weller, J. Stöhr, R. Nakajima, A. Carl, M. G. Samant, C. Chappert, R. Mégy, P. Beauvillain, P. Veillet, and G. A. Held, Phys. Rev. Lett. **75**, 3752 (1995).
[31]J. M. Shaw, H. T. Nembach, T. J. Silva, S. E. Russek, R. Geiss, C. Jones, N. Clark, T. Leo, and D. J. Smith, Phys. Rev. B **80**, 184419 (2009).
[32]H. T. Nembach, T. J. Silva, J. M. Shaw, M. L. Schneider, M. J. Carey, S. Maat, and J. R. Childress, Phys. Rev. B **84**, 054424 (2011).
[33]B. Heinrich, J. F. Cochran, and R. Hasegawa, J. Appl. Phys. **57**, 3690 (1985).
[34]M. Farle, Rep. Prog. Phys. **61**, 755 (1998).
[35]R. D. McMichael, D. J. Twisselmann, and A. Kunz, Phys. Rev. Lett. **90**, 227601 (2003).
[36]T. D. Rossing, J. Appl. Phys. **34**, 995 (1963).
[37]R. D. McMichael and P. Krivosik, IEEE Trans. Magn. **40**, 2 (2004).
[38]N. Mo, J. Hohlfeld, M. ul Islam, C. S. Brown, E. Girt, P. Krivosik, W. Tong, A. Rebei, and C. E. Patton, Appl. Phys. Lett. **92**, 022506 (2008).
[39]T. Thomson, G. Hu, and B. D. Terris, Phys. Rev. Lett. **96**, 257204 (2006).
[40]J. M. Shaw, W. H. Rippard, S. E. Russek, T. Reith, and C. M. Falco, J. Appl. Phys. **101**, 023909 (2007).
[41]O. Ozatay, T. Hauet, S. H. Florez, J. A. Katine, A. Moser, J. U. Thiele, L. Folks, and B. D. Terris, Appl. Phys. Lett. **95**, 3 (2009).
[42]J. Foros, G. Woltersdorf, B. Heinrich, and A. Brataas, J. Appl. Phys. **97**, 10A714 (2005).
[43]P. Bruno, Phys. Rev. B **39**, 865 (1989).
[44]G. H. O. Daalderop, P. J. Kelly, and M. F. H. Schuurmans, Phys. Rev. B **42**, 7270 (1990).
[45]H. Nemoto and Y. Hosoe, J. Appl. Phys. **97**, 10J109 (2005).
[46]Z. Celinski, B. Heinrich, and J. F. Cochran, J. Appl. Phys. **70**, 5870 (1991).
[47]R. J. Hicken, A. J. R. Ives, D. E. P. Eley, C. Daboo, J. A. C. Bland, J. R. Childress, and A. Schuhl, Phys. Rev. B **50**, 6143 (1994).
[48]E. E. Fullerton, D. Stoeffler, K. Ounadjela, B. Heinrich, Z. Celinski, and J. A. C. Bland, Phys. Rev. B **51**, 6364 (1995).
[49]Y. Takahashi, Phys. Rev. B **56**, 8175 (1997).
[50]E. E. Fullerton, J. S. Jiang, M. Grimsditch, C. H. Sowers, and S. D. Bader, Phys. Rev. B. **58**, 12193 (1998).
[51]B. Heinrich, G. Woltersdorf, R. Urban, and E. Simanek, J. Appl. Phys. **93**, 7545 (2003).
[52]See Supplemental Material at http://link.aps.org/supplemental/10.1103/PhysRevB.85.054412 for evaluation of effective thickness.
[53]See Supplemental Material at http://link.aps.org/supplemental/10.1103/PhysRevB.85.054412 for 1-d diffusive approximation.